

Baryogenesis via flavoured leptogenesis in a minimal type-II seesaw model

Sreerupa Chongdar* and Sasmita Mishra†

Department of Physics and Astronomy,

National Institute of Technology Rourkela, Sundargarh, Odisha, India, 769008

Abstract

We study baryogenesis via leptogenesis in an extension of the Standard Model by adding one right-handed neutrino and one triplet scalar. These heavy particles contribute to the generation of tiny neutrino mass through seesaw mechanism. The contribution of the heavy particles to the neutrino masses is inversely proportional to their corresponding masses. Considering leptogenesis is achieved by the decay of the right-handed neutrino, the new source of CP asymmetry comes solely from the decay of the right-handed neutrino with one-loop vertex diagram involving the triplet scalar. The predictiveness of the model is enhanced by introducing Fritzsch-type textures for the neutrino mass matrix and charged lepton mass matrix. We execute the parameter space study following the latest neutrino oscillation data. We study baryogenesis via leptogenesis in the two-flavoured regime, using the zero textures, and show that there is an enhancement in baryon asymmetry as compared to the unflavoured regime. For two-flavour leptogenesis we consider the suitable temperature regime $T \subset [10^{10}, 10^{11}]$ GeV. We also study the common correlation of CP violation between low and high-energy regimes using the geometrical description of CP violation in terms of unitarity triangle.

*Electronic address: 518PH1002@nitrkl.ac.in

†Electronic address: mishras@nitrkl.ac.in

I. INTRODUCTION

The two enigmatic problems of non-zero neutrino mass and baryon asymmetry of the Universe find a common solution in the Standard Model (SM) augmented with a certain choice of additional heavy fields. Through the seesaw mechanism one can provide a possible theoretical explanation of nonzero neutrino mass, confirmed by the experimental observation of neutrino flavour oscillation [1]. The observed baryon asymmetry of the Universe (BAU) could also be explained through leptogenesis [2] via out-of-equilibrium decay of the same heavy fields taking part in the seesaw mechanism. The former is one low-energy observation (after electroweak symmetry breaking) whereas the latter, a high-energy phenomenon (before electroweak symmetry breaking). Thus seesaw mechanism provides a nontrivial link between the generation of light neutrino mass and baryogenesis through leptogenesis. In this work, we study the generation of BAU through flavoured leptogenesis in the minimally extended SM by one fermion singlet and one scalar triplet. The phenomena of CP violation is inevitable both in neutrino oscillation and leptogenesis. We also establish a link between low- and high-energy CP violations.

One of the famous frameworks of neutrino mass generation via seesaw mechanism and leptogenesis via out-of-equilibrium decay of a heavy beyond SM field is the one where the SM is extended with heavy right-handed neutrinos. One needs more than just one right handed neutrino to account for light neutrino mass generation, compatible with experimental data and leptogenesis. The addition of right-handed neutrinos is also consistent with the theories inspired by Grand Unification such as Left-right symmetry [3–5], Pati-Salam [6] and SO(10) [7, 8]. However, in such theories, heavy fields such as scalar triplets and fermion triplets arise naturally and can establish the connection between light neutrino mass generation via seesaw mechanism and leptogenesis.

Keeping minimal extension of the SM in mind, we study a minimal type-II seesaw model, where the SM is extended with one $SU(2)_L$ triplet scalar, Δ and one right-handed singlet fermion, N . So in our study, there are two mass scales involved: the mass of the right-handed singlet, M and that of scalar triplet, M_Δ . While both the fields contribute to light neutrino mass via seesaw mechanism, considering hierarchical mass limits, the out-of-equilibrium decay of one field is responsible for creating lepton asymmetry and hence BAU via leptogenesis. The requirement of CP violation being essential for baryogenesis via

leptogenesis [9], it is possible to produce CP violation in two ways in such a model. The vertex diagram involving one right-handed neutrino and one triplet scalar can be of two types, depending on the relative hierarchy of their masses:

1. If we have the triplet scalar as the lightest seesaw state ($M_\Delta \ll M$), then the decay of the triplet scalar dominates the CP asymmetry in the presence of a virtual right-handed neutrino present in the vertex diagram.
2. If the right-handed neutrino is lighter than the triplet scalar ($M \ll M_\Delta$), the CP asymmetry is produced predominantly from the decay of the right-handed neutrino in the presence of a virtual triplet scalar in the vertex diagram.

In the SM, considering there are not so light scalars we choose to work in the hierarchy $M \ll M_\Delta$. In a model with n number of right-handed neutrinos and one triplet scalar, the neutrino mass can be generated from two sources,

$$m_\nu = m_\nu^{(I)} + m_\nu^{(II)}, \quad (1)$$

where $m_\nu^{(I)}$ is the right-handed neutrino contribution coming from the type-I seesaw mechanism, and $m_\nu^{(II)}$ is the triplet scalar contribution coming from the type-II seesaw mechanism. If we consider the lightest right-handed neutrino N_1 to be the lightest seesaw state, then the CP asymmetry can be obtained from the decay of N_1 in the presence of the other right-handed neutrinos (N_2, \dots, N_n) or the triplet scalar Δ in the vertex diagram. There is no one-to-one correspondence by each seesaw state, between the amount of contribution to neutrino mass and CP asymmetry (as the neutrino mass matrix is a 3×3 complex matrix, not a number). But the contribution of the seesaw states to the production of CP asymmetry is found to be proportional to their respective contribution to the neutrino mass generation [10]. In that case, in the limit, $m_\nu^{(I)} \gg m_\nu^{(II)}$, the contribution of the triplet scalar in the production of CP asymmetry can be safely ignored. However, in a minimal type-II seesaw model, the CP asymmetry can be obtained only from the one-loop vertex diagram involving the triplet scalar as there is only one right-handed neutrino. So we will consider the contribution of triplet scalar in the CP asymmetry production.

In the study of baryogenesis through leptogenesis flavour effects are known to induce some novel feature as compared to unflavoured case especially due to the nature of wash-out effects along different directions in flavour space. At higher temperature, $T \gtrsim 10^{12}$ GeV, the charged

lepton flavours (e, μ, τ) are out of thermal equilibrium and thus indistinguishable. In this case, the leptogenesis can be successfully expressed in an unflavoured regime. However, at a temperature $T \lesssim 10^{12}$ GeV, the processes induced by τ -Yukawa are in thermal equilibrium. It breaks the coherence between τ -lepton and the other two leptons (e, μ) . The lepton asymmetries are expressed through Y_{Δ_a} and Y_{Δ_τ} in this temperature range, where $a = e + \mu$ is the superposition of the flavours e and μ . Further below $T \sim 10^9$ GeV, the interactions induced by the μ -Yukawa are in thermal equilibrium, completely breaking the flavour coherence. So, leptogenesis needs to be studied in terms of fully flavoured lepton asymmetries, Y_{Δ_e} , Y_{Δ_μ} , and Y_{Δ_τ} at temperature $T \lesssim 10^9$ GeV.

In seesaw models, generally, there are many free parameters as long as the coupling matrices are concerned. There are not enough experimental constraints to fix the parameters. The number of free parameters can be reduced by imposing texture zeros in the coupling matrices. Often they are motivated by imposing new symmetries on the particle content of the model. In this way, the model becomes predictive by fitting the parameters to low-energy neutrino data. Taking Fritzsch-type textures [11–15] into account we show that the BAU can be enhanced to comply with observational value, considering flavoured effects as compared to unflavoured case. This feature is helpful in bringing down the scale of leptogenesis. We study the two-flavoured leptogenesis in the temperature range $T \sim [10^{10}, 10^{11}]$ GeV. We find that the lepton asymmetries obtained through leptogenesis can lead to baryon asymmetry of the order $\sim 10^{-10}$, and the proper flavour consideration enhances the production of baryon asymmetry. It is believed that the CP violation in low-energy (e.g. neutrino oscillation) and high-energy regimes (e.g. leptogenesis) are in general not related. Using a geometrical interpretation of CP violation at low-energy, we also show a common link between low and high energy CP violation in this setup.

The paper is organized as follows. In section (II), a minimal type-II neutrino mass model is introduced. In section (II A), a detailed parameter space study of the neutrino mass matrix elements is carried out, which covers the diagonalization of matrices and the interesting correlation among different mixing angles arising from the model. The allowed parameter space indicated in this section is further used to obtain CP asymmetry parameters. In section (III), the processes like baryogenesis and leptogenesis are discussed from a cosmological point of view. Section (III A) contains the results and discussions. It gives a comparative study among these regimes of leptogenesis, generically judged based on different right-handed

neutrino masses M . The common origin of CP violations in low- and high-energy sectors is analyzed in section (IV). Finally, in section (V), we give our conclusions of the study.

II. NEUTRINO MASS MODEL

With addition of a triplet scalar, Δ and n -number of right-handed Majorana neutrinos, N_i ($i = 1, \dots, n$), the extended SM Lagrangian can be written as

$$-\mathcal{L} \supset Y_{l\alpha\beta} \bar{L}_\alpha l_{R\beta} \phi + Y_{\nu\alpha i} \bar{L}_\alpha N_i \phi + \frac{1}{2} M_i \bar{N}_i N_i + Y_{\Delta\alpha\beta} \bar{L}_\alpha^C i\tau_2 \Delta L_\beta - \mu \phi^T i\tau_2 \Delta \phi + M_\Delta^2 \text{Tr} \Delta^\dagger \Delta + \text{h.c.}, \quad (2)$$

where $L_\alpha = (\nu_\alpha, l_\alpha)^T$ and $l_{R\beta}$, ($\alpha, \beta = e, \mu, \tau$) are the left- and right-handed SM leptons respectively. The SM Higgs doublet is represented as $\phi = (\phi^0, \phi^-)^T$. The triplet scalar, Δ can be represented in $SU(2)_L$ adjoint representation as,

$$\Delta = \begin{pmatrix} \frac{\delta^+}{\sqrt{2}} & \delta^{++} \\ \delta^0 & -\frac{\delta^+}{\sqrt{2}} \end{pmatrix}.$$

The Dirac-type Yukawa coupling matrix of the right-handed neutrinos and charged leptons with the SM leptons and Higgs scalar are represented as Y_ν and Y_l respectively. The coupling matrix, Y_Δ is a 3×3 Majorana-type Yukawa coupling matrix of the triplet scalar with the SM lepton doublets. After electroweak symmetry breaking, due to the vacuum expectation value (vev) developed by the neutral component of the doublet Higgs, $v = \langle \phi_0 \rangle$, the neutral component of Δ also acquires a vev, $v_\Delta = \langle \delta_0 \rangle \simeq \frac{\mu^* v^2}{M_\Delta^2}$. The triplet vev, v_Δ is seesaw suppressed for heavy triplet scalar. Once the heavy degrees of freedom are integrated out, as a consequence, there are two sources of light neutrino masses,

$$m_\nu = m_\nu^{(I)} + m_\nu^{(II)} = -Y_\nu^* \frac{1}{M} Y_\nu^\dagger v^2 + 2Y_\Delta v_\Delta. \quad (3)$$

The first and second terms are mass terms due to type-I and II seesaw induced masses respectively, with $v = 174$ GeV. The low-energy neutrino oscillation experiments provide data for six parameters: three mixing angles, two mass-squared differences, and one CP violation phase. In our model, the Dirac-type Yukawa coupling for right-handed neutrinos has 6 (3 moduli and 3 phases for one right-handed neutrino) and the Majorana-type Yukawa which is complex symmetric, has 12 (6 moduli and 6 phases) independent parameters. In order to make the model predictive we assume the Fritzsch-type textures [11–15] of charged

lepton mass matrix, m_l and triplet scalar induced neutrino mass matrix, $m_\nu^{(II)}$. Following the same texture for both,

$$m_l = v \begin{pmatrix} 0 & C_l e^{i\alpha_l} & 0 \\ C_l e^{i\alpha_l} & 0 & B_l e^{i\beta_l} \\ 0 & B_l e^{i\beta_l} & A_l e^{i\gamma_l} \end{pmatrix}, \quad (4)$$

and

$$m_\nu^{(II)} = v_\Delta \begin{pmatrix} 0 & C_\nu e^{i\alpha_\nu} & 0 \\ C_\nu e^{i\alpha_\nu} & 0 & B_\nu e^{i\beta_\nu} \\ 0 & B_\nu e^{i\beta_\nu} & A_\nu e^{i\gamma_\nu} \end{pmatrix}. \quad (5)$$

Such textures arise in left-right symmetric models, where right-handed neutrinos and triplet scalars arise naturally and were studied in Ref. [16]. Also, in the construction of models based on Froggatt-Nielsen mechanism [17], texture zeros arise in the neutrino Yukawa coupling due to the assignment of different charges under an additional symmetry to particles of different generations. The consequences of texture zeros in (1, 1), (1, 2) and (1, 3) positions of Yukawa matrix have interesting consequences in flavoured leptogenesis as shown in Ref.[18]. For example in the case of texture zero in (1, 1) position, e -CP asymmetry is weakly washed out while the μ - and τ -CP asymmetries are strongly washed out. In the quark sector, the simultaneous presence of zeros in the (1, 1) elements of symmetric up and down quark mass matrices leads to the prediction of Cabibbo angle $\theta_C \simeq \sqrt{m_d/m_s}$ [19].

In our case, we have one right-handed neutrino. So the corresponding Yukawa coupling matrix is a column matrix, which can be set as [20],

$$Y_\nu = iy_0 (0, r, 1)^T. \quad (6)$$

The purpose of introducing imaginary unit i is to cancel the minus sign of the type-I term for convenience. The appearance of zero in the (1, 1) position of the above Yukawa matrix ensures two-zero texture in the total light neutrino mass matrix as can be seen in the subsequent equation. Now using the equations (5) and (6) in Eq.(3), the neutrino mass matrix turns out to be

$$m_\nu = m_0 \begin{pmatrix} 0 & \hat{C}_\nu e^{i\alpha_\nu} & 0 \\ \hat{C}_\nu e^{i\alpha_\nu} & r^2 & r + \hat{B}_\nu e^{i\beta_\nu} \\ 0 & r + \hat{B}_\nu e^{i\beta_\nu} & 1 + \hat{A}_\nu e^{i\gamma_\nu} \end{pmatrix}. \quad (7)$$

Here $m_0 \equiv v^2 y_0^2 / M$ and $\hat{A}_\nu \equiv v_\Delta A_\nu / m_0$ and similarly for \hat{B}_ν and \hat{C}_ν .

A. Parameter space determination by confronting with neutrino data

To study the neutrino mass generation and to produce optimum CP asymmetry from the neutrino mass model, we need to study the parameter space offered by the model.

There are three important steps to be followed for diagonalizing the matrices and make a connection with experimental observations [21, 22].

1. In the first step the charged and neutral lepton mass matrices are decomposed in terms of diagonal phase matrix, $P_{l,\nu}$ and real symmetric matrix, $\bar{m}_{l,\nu}$ so that

$$m_{l,\nu} = P_{l,\nu}^T \bar{m}_{l,\nu} P_{l,\nu}, \quad (8)$$

where

$$P_{l,\nu} = \begin{pmatrix} e^{i\theta_{l,\nu}} & 0 & 0 \\ 0 & e^{i\phi_{l,\nu}} & 0 \\ 0 & 0 & e^{i\psi_{l,\nu}} \end{pmatrix}. \quad (9)$$

2. In the second step the real symmetric matrix, $\bar{m}_{l,\nu}$ is diagonalized following unitary transformation:

$$U_l^T \bar{m}_l U_l = \text{Diag}(m_e, m_\mu, m_\tau), \quad U_\nu^T \bar{m}_\nu U_\nu = \text{Diag}(m_1, m_2, m_3), \quad (10)$$

where m_e, m_μ and m_τ are the masses of e, μ and τ leptons respectively. The mass eigenvalues of the light neutrino mass matrix are represented as m_1, m_2 and m_3 .

3. The lepton flavour mixing matrix, V then arises from the mismatch between the diagonalization of the charged and neutral mass matrices: $V = U_l^T (P_l^* P_\nu) U_\nu^*$. The elements of the matrix can be written as

$$V_{pq} = U_{l1p} U_{\nu 1q}^* e^{i\theta} + U_{l2p} U_{\nu 2q}^* e^{i\phi} + U_{l3p} U_{\nu 3q}^* e^{i\psi}, \quad (11)$$

where $p \equiv (e, \mu, \tau)$, $q \equiv (1, 2, 3)$. The phases are defined as, $\theta = (\theta_\nu - \theta_l)$, $\phi = (\phi_\nu - \phi_l)$, $\psi = (\psi_\nu - \psi_l)$. The elements of U_ν and U_l are given in the appendices (A) and (B).

4. The elements of the mixing matrix V depends on only two combinations of three phases, (θ, ϕ, ψ) as the overall phase of V has nothing to do with experimental observable. The elements of the matrices $U_{l,\nu}$ also depend on the mass ratios of the charged

and neutral leptons, as given below,

$$x_l = \frac{m_e}{m_\mu}, \quad y_l = \frac{m_\mu}{m_\tau}, \quad (12)$$

$$x_\nu = \frac{m_1}{m_2}, \quad y_\nu = \frac{m_2}{m_3}. \quad (13)$$

The charged lepton ratios x_l, y_l are now determined with better accuracy, as

$$x_l \simeq 0.00484, \quad y_l \simeq 0.0594. \quad (14)$$

So, there are only four free parameters (two phases and x_ν and y_ν) that can be constrained from neutrino oscillation data.

The three mixing angles θ_{ij} of the neutrino oscillation parameters can be expressed in terms of the lepton flavour mixing matrix V , as follows:

$$\sin^2 2\theta_{12} = 4 |V_{e1}|^2 |V_{e2}|^2, \quad (15)$$

$$\sin^2 2\theta_{23} = 4 |V_{\mu 3}|^2 (1 - |V_{\mu 3}|^2), \quad (16)$$

$$\sin^2 2\theta_{13} = 4 |V_{e3}|^2 (1 - |V_{e3}|^2). \quad (17)$$

The parameter space of $[x_\nu, y_\nu]$ can be restricted by the bounds on mixing angles. The experimental constraints are given by [23],

$$31.27^\circ < \theta_{12} < 35.87^\circ, \quad 39.7^\circ < \theta_{23} < 50.9^\circ, \quad (18)$$

$$8.25^\circ < \theta_{13} < 8.98^\circ, \quad 144^\circ < \delta < 350^\circ. \quad (19)$$

Even though the Dirac CP phase δ is bounded as

$$144^\circ < \delta < 350^\circ, \quad (20)$$

we have used the full range of $\delta \sim [0 : 360^\circ]$ for the parameter space study. The latest bounds on the two mass-squared differences are given by

$$\begin{aligned} 6.82 \times 10^{-5} \text{ eV}^2 &< \Delta m_{21}^2 < 8.04 \times 10^{-5} \text{ eV}^2, \\ 2.430 \times 10^{-3} \text{ eV}^2 &< \Delta m_{31}^2 < 2.593 \times 10^{-3} \text{ eV}^2. \end{aligned} \quad (21)$$

Once the values of x_ν and y_ν are constrained the absolute values of three neutrino masses can be found by using the mass-squared differences,

$$\Delta m_{21}^2 = m_2^2 - m_1^2 = m_2^2 |1 - x_\nu^2|, \quad \Delta m_{31}^2 = m_3^2 - m_1^2 = m_3^2 |1 - y_\nu^2|. \quad (22)$$

In order to diagonalize the charged lepton and neutrino mass matrices given in equations (4) and (7) and determine the parameter space using experimental data we follow the steps laid above. In order to write the lepton mass matrices m_l and m_ν in factorized form as given in Eq.(8), we make two assumptions here: $r = \sqrt{m_2/m_0}$ and $\arg(1 + \hat{A}_\nu e^{i\gamma_\nu}) = 2\arg(r + \hat{B}_\nu) e^{i\beta_\nu}$ [21] and then obtain

$$\hat{A}_\nu = \left[\frac{(m_3 - m_1)^2}{m_0^2} - \sin^2 \gamma_\nu \right]^{\frac{1}{2}} - \cos \gamma_\nu, \quad (23)$$

$$\hat{B}_\nu = \left[\frac{m_1 m_3 (m_3 - m_1 - m_2)}{m_0^2 (m_3 - m_1)} - r^2 \sin^2 \beta_\nu \right]^{\frac{1}{2}} - r \cos \beta_\nu, \quad (24)$$

$$\hat{C}_\nu = \left[\frac{m_1 m_2 m_3}{m_0^2 (m_3 - m_1)} \right]^{\frac{1}{2}}. \quad (25)$$

Similarly, the elements of the charged lepton mass matrix, shown in Eq.(4), can be expressed in terms of three charged lepton masses m_e , m_μ and m_τ .

$$A_l = (m_\tau - m_\mu + m_e), \quad (26)$$

$$B_l = \left[\frac{(m_\mu - m_e)(m_\tau - m_\mu)(m_e - m_\tau)}{(m_\tau - m_\mu + m_e)} \right]^{\frac{1}{2}}, \quad (27)$$

$$C_l = \left[\frac{m_e m_\mu m_\tau}{(m_\tau - m_\mu + m_e)} \right]^{\frac{1}{2}}. \quad (28)$$

In order to determine the parameter space of x_ν and y_ν we assume the general range of the lightest neutrino mass in normal hierarchy (NH), as $m_1 \sim [0.001 : 0.05]$ eV. Hence, the other neutrino masses can be calculated directly from Eq.(22). The plot in Fig.(1) shows how different bounds restrict the parameter space of x_ν and y_ν . In Fig.(1), the scattered points represent the allowed values of x_ν and y_ν that satisfy total neutrino mass $\Sigma = m_1 + m_2 + m_3 < 0.12$ eV [24], mass-squared differences and mixing angles as given in equations (18) - (21). One can see a commonly allowed parameter space as the allowed ranges of x_ν and y_ν are given by,

$$x_\nu \sim [0.80 - 0.90], \quad y_\nu \sim [0.30 - 0.35]. \quad (29)$$

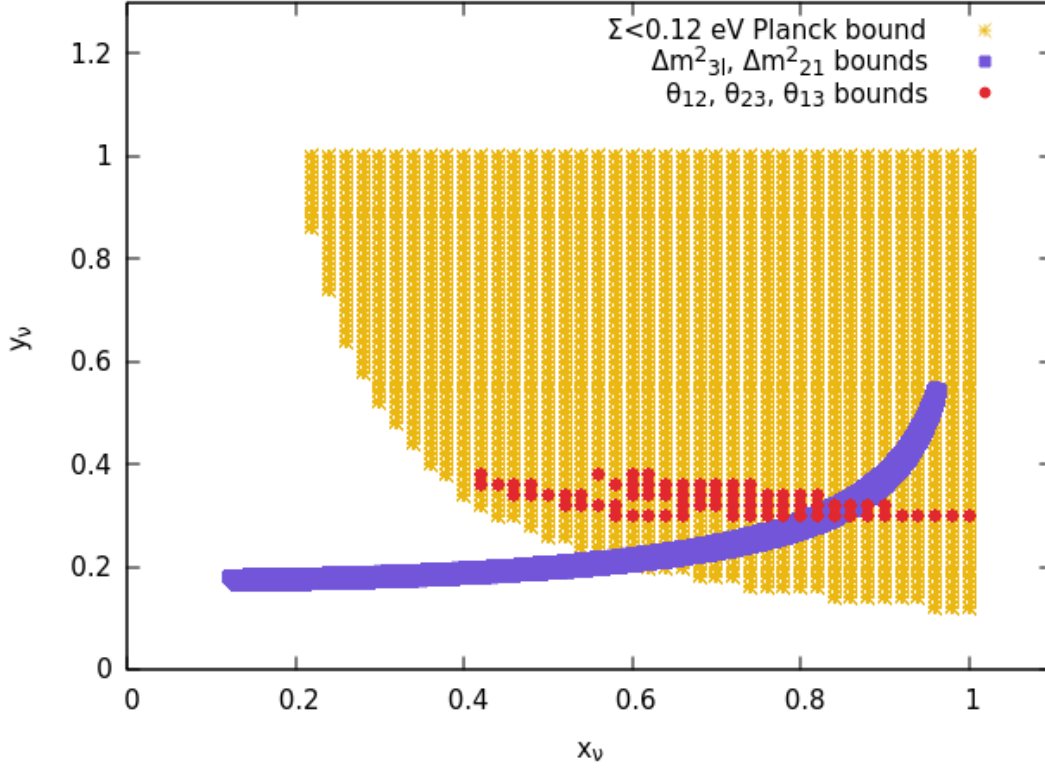


FIG. 1: The figure is a representation of the determination of parameter space of $[x_\nu, y_\nu]$. The blue region is bounded by the constraints coming from two mass-squared differences, $\frac{\Delta m_{21}^2}{10^{-5}}(eV^2) \in [6.82, 8.04]$, and $\frac{\Delta m_{31}^2}{10^{-3}}(eV^2) \in [2.430, 2.593]$. The yellow region is bounded by the Planck constraint on the total neutrino mass $\Sigma = m_1 + m_2 + m_3 < 0.12$ eV. The red region is bounded by the constraints coming from the three mixing angles $\theta_{12} \in [31.27^\circ, 35.87^\circ]$, $\theta_{23} \in [39.7^\circ, 50.9^\circ]$, and $\theta_{13} \in [8.25^\circ, 8.98^\circ]$. The intersection of these three regions is the small allowed parameter space for $x_\nu \in [0.80 - 0.90]$ and $y_\nu \in [0.30 - 0.35]$.

We shall use these ranges to estimate the CP asymmetry parameter for the study of leptogenesis. The parameter space for the neutrino mass matrix elements \hat{A}_ν , \hat{B}_ν and \hat{C}_ν can be further constrained using the latest neutrino oscillation parameter data using equations (23 - 25), as the model contributes to the formation of baryon asymmetry through these matrix elements.

III. BARYOGENESIS AND LEPTOGENESIS

The baryon asymmetry of the Universe, $\eta_B = (n_B - n_{\bar{B}})/n_\gamma$ is constrained from the Big Bang Nucleosynthesis (BBN) and Cosmic Microwave Background Radiation (CMBR) data [25], and is given by,

$$4.7 \times 10^{-10} \leq \eta_B \leq 6.5 \times 10^{-10}, \quad (30)$$

where n_B , $n_{\bar{B}}$, and $n_\gamma = \frac{2\zeta(3)}{\pi^2}T^3$ denote the number densities of baryons, antibaryons, and gamma photons respectively. Theoretically, baryogenesis through leptogenesis [26] provides a framework for generating the required BAU following three Sakharov's conditions [9]. In the seesaw model under consideration, they are satisfied as follows: (i) The lepton number violation comes into the scenario from the decay of right-handed neutrino considering neutrinos as Majorana particles. (ii) CP violation is ensured from the interference of the tree-level and one-loop diagrams of the decay of the right-handed neutrino. (iii) The out-of-equilibrium condition is achieved by determining the particle asymmetries, while considering the decay and inverse decay processes in an expanding early Universe through a set of Boltzmann equations. The lepton asymmetry is converted to the baryon asymmetry through $B + L$ violating Sphaleron processes [27].

If the temperature is as high as $T \sim 10^{12}$ GeV or more, the individual flavours of the leptons do not appear to be of much importance, and in this case, solving a set of flavour-independent or unflavoured Boltzmann equations proves to be sufficient to study the leptogenesis. On the other hand, in the temperature range $T \subset [10^{10}, 10^{12}]$ GeV, τ -Yukawa interactions are faster than the rate of expansion of the Universe, making τ -leptons decouple from the flavour coherent lepton state. Hence, it is essential to study leptogenesis in a two-flavoured regime. Below $T \sim 10^9$ GeV, the μ -leptons decouple and completely break down the flavour coherence of the leptons. Hence, the study of leptogenesis requires three-flavour consideration. So we have a set of flavour-independent and flavour-specific Boltzmann equations given below, and we solve it numerically to obtain the unflavoured, and flavoured lepton asymmetries. As mentioned before, the Boltzmann equations [20, 28–30] take care of the dynamics of particle abundancies, taking care of the production of CP asymmetries and washing out of the asymmetry due to the interplay between decay and inverse decay processes. These equations are expressed in terms of particle asymmetries of species x , $Y_x = \frac{n_x}{s}$

where n_x is the number density and s is the entropy density.

$$\frac{dY_N}{dz} = -\frac{\gamma_D}{sHz} \left(\frac{Y_N}{Y_N^{eq}} - 1 \right) \quad (31)$$

$$\frac{dY_{\Delta_i}}{dz} = -\frac{\gamma_D}{sHz} \left[\left(\frac{Y_N}{Y_N^{eq}} - 1 \right) \epsilon_i + K_0^i \sum_j \frac{1}{2} (C_{ij}^l + C_j^H) \frac{Y_{\Delta_j}}{Y_l^{eq}} \right] \quad (32)$$

where $z = \frac{M}{T}$, the decay and inverse decay rate of the right handed neutrino ($N \rightarrow l\phi$), $\gamma_D = DsHzY_N^{eq}$, $D = Kz \frac{K_1(z)}{K_2(z)}$, s is the entropy density, K_1 and K_2 are modified Bessel functions, Y_{Δ_i} being the i-flavoured lepton asymmetry, $Y_N^{eq} = \frac{45}{2\pi^4 g_*} z^2 K_2(z)$, and $Y_l^{eq} = \frac{15}{4\pi^2 g_*}$. The decay or wash-out parameter,

$$K \equiv \frac{\sum_\alpha \Gamma(N \rightarrow L_\alpha \phi)}{H(M)} = \frac{\tilde{m}}{m_*}, \quad (33)$$

where \tilde{m} is the effective neutrino mass $\tilde{m} \equiv \frac{(Y^\dagger Y)_{11} v^2}{M}$ and is proportional to the total decay rate of the right-handed neutrino. $H(M)$ is the Hubble parameter evaluated at a temperature $T = M$; $m_* \sim 10^{-3}$ eV is equilibrium neutrino mass. We have considered the case of strong wash-out ($\tilde{m} > m_*$) for our study. K_0^i are the flavour projection operators where $i = a, \tau$ in two-flavour configuration, and $i = e, \mu, \tau$ in three-flavour configuration. It can be expressed as [18, 29, 31–34],

$$K_0^i = \frac{(Y^*)_{i1} (Y)_{i1}}{(Y^\dagger Y)_{11}}. \quad (34)$$

The importance of flavour projection operators is discussed further in the appendix (C).

In the case of flavour-independent lepton asymmetry, Eq.(32) can be written as

$$\frac{dY_\Delta}{dz} = -\frac{\gamma_D}{sHz} \left[\left(\frac{Y_N}{Y_N^{eq}} - 1 \right) \epsilon + \frac{1}{2} \frac{Y_\Delta}{Y_l^{eq}} \right], \quad (35)$$

where Y_Δ represents the unflavoured lepton asymmetry.

In this study, the lepton number violating decays of the heavy states introduced in the seesaw mechanism act as new sources of CP violation. For our model, one right-handed neutrino N and one heavier triplet scalar Δ are chosen as the two heavy states. The lepton number violating effects produced by the heavier state get washed out due to the same produced by the lighter state. So, here the CP asymmetry is getting generated from the decay of the right-handed Majorana neutrino, with the assumption $M \ll M_\Delta$. The CP asymmetry can be calculated from the interaction of ordinary tree-level decay and the three diagrams shown in Fig.(2). The first two figures are self-energy and vertex diagrams

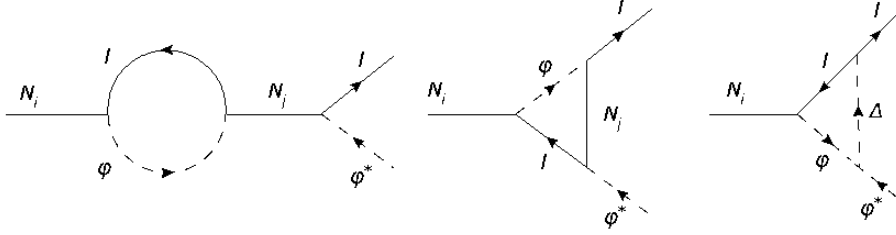


FIG. 2: The one-loop Feynman diagrams of N_i decay in a model with n number of right-handed neutrinos and one triplet, Δ . In our case, we have one right-handed neutrino, so CP violation comes from the interference of tree-level diagram with the third diagram.

mediated by one extra heavy right-handed neutrino. Nevertheless, there is only one right-handed neutrino in the model under consideration. So the third figure representing the vertex diagram mediated by the Higgs triplet scalar Δ contributes to the generation of CP asymmetry. In the temperature range $T > 10^{12}$ GeV, the lepton flavours states can be approximated as a single or unflavoured state. In that temperature range, we write the flavour-independent CP asymmetry parameter as [20]

$$\epsilon_N^\Delta \simeq \frac{3}{16\pi} \frac{M}{v^2} \frac{\sum_{\alpha\beta} \text{Im} \left[Y_{1\alpha}^\dagger Y_{1\beta}^\dagger (m_\nu^{(II)*})_{\alpha\beta} \right]}{(Y^\dagger Y)_{11}}. \quad (36)$$

Again, for temperature $T \ll 10^{12}$ GeV, the lepton flavours become distinguishable, and the flavour consideration becomes important. Then the flavour-specific CP asymmetry parameter can be written as [35, 36]

$$\epsilon_{N,\alpha}^\Delta \simeq \frac{3}{16\pi} \frac{M}{v^2} \frac{\sum_{\beta} \text{Im} \left[Y_{1\alpha}^\dagger Y_{1\beta}^\dagger (m_\nu^{(II)*})_{\alpha\beta} \right]}{(Y^\dagger Y)_{11}}. \quad (37)$$

For simplicity, we write the unflavoured CP asymmetry as ϵ and the flavour specific CP asymmetry as ϵ_i , where $i = e, \mu, \tau$ or $a = e + \mu$. From Eq.(36), we obtain the expression of the unflavoured CP asymmetry parameter, using the neutrino mass matrix elements

$$\epsilon = \frac{3}{16\pi} \frac{M}{v^2 (1 + r^2)} m_0 \left(\hat{A}_\nu \sin \gamma_\nu + 2r \hat{B}_\nu \sin \beta_\nu \right). \quad (38)$$

From Eq.(37), we can further obtain the two-flavoured CP asymmetries ϵ_a , ($a = e + \mu$) and ϵ_τ ,

$$\epsilon_a = \frac{3}{16\pi} \frac{M}{v^2 (1 + r^2)} r m_0 \hat{B}_\nu \sin \beta_\nu,$$

and

$$\epsilon_\tau = \frac{3}{16\pi} \frac{M}{v^2(1+r^2)} m_0 \left(r \hat{B}_\nu \sin \beta_\nu + \hat{A}_\nu \sin \gamma_\nu \right), \quad (39)$$

which is relevant in the temperature range $T > 10^9$ GeV.

The CP asymmetry parameters are to be determined from the model to further investigate different lepton asymmetries through a set of Boltzmann equations. In the temperature range $10^{11} \text{ GeV} \lesssim T \lesssim 10^{12} \text{ GeV}$, under two-flavoured leptogenesis regime,

$$C^H = \frac{1}{230} (41, 56), \quad (40)$$

$$C^l = \frac{1}{460} \begin{pmatrix} 196 & -24 \\ -9 & 156 \end{pmatrix}. \quad (41)$$

Finally, we can estimate the baryon asymmetry after solving the suitable set of Boltzmann equations numerically and obtain the lepton asymmetry. In the case of unflavoured leptogenesis, we use the expression,

$$\eta_B = -7.04 \times Y_B, \quad Y_B = -1.38 \times 10^{-3} \epsilon \eta, \quad (42)$$

to calculate baryon asymmetry [28], where

$$\eta = \frac{Y_\Delta(z \gg 1)/\epsilon}{Y_N^{eq}(0)}, \quad (43)$$

is known as the efficiency factor [37]. In the case of flavoured leptogenesis, the expression of baryon asymmetry given in Eq.(42) is replaced by [28]

$$\eta_B = -7.04 \times Y_B, \quad Y_B = -1.38 \times 10^{-3} \sum_i Y_{\Delta_i}(z \gg 1). \quad (44)$$

In the next subsection we make a quantitative analysis of the BAU in the model.

A. Baryon asymmetry determination: Result

In this section, we make quantitative analysis of baryon asymmetry by calculating the CP asymmetry and solving the set of Boltzmann equations, both for unflavoured and flavoured leptogenesis. The CP asymmetries are calculated by using equations (38)- (39) for unflavoured and flavoured leptogenesis respectively. Similarly the corresponding set of Boltzmann equations (31), (32) and (35) are taken into account to calculate the final BAU using

equations (42) and (44). It is known that the generation of BAU can be enhanced by taking flavour effects into account over unflavoured leptogenesis. Here, we show that Fritzsch-type textures can be used to verify the above characteristic of leptogenesis mechanism. So an integrated scenario of generation of baryon asymmetry and experimentally compatible values of neutrino mixing parameters can be achieved in this framework.

Although unflavoured leptogenesis is viable above temperature $T \gtrsim 10^{12}$ GeV, we make comparison between unflavoured and flavoured leptogenesis by bringing down the leptogenesis scale to $10^{10} - 10^{11}$ GeV, suitable for studying two-flavoured leptogenesis. In order to study the cases of unflavoured and two-flavoured leptogenesis, we choose different values of M in the range $4 \times 10^{10} \text{ GeV} \leq M \leq 5 \times 10^{11} \text{ GeV}$, and four benchmark sets are formed corresponding to those M values. For each benchmark set, the values of neutrino mass eigenvalue m_1 , phases γ_ν , β_ν , and y_0 are made to be fixed for calculating the CP asymmetry. The values are consistent with the oscillation data. Using the chosen values for these parameters the effective neutrino mass $\tilde{m} = \frac{(Y^\dagger Y)_{11} v^2}{M} = \frac{y_0^2 (1+r^2)}{M}$, neutrino mass matrix elements \hat{A}_ν , \hat{B}_ν , \hat{C}_ν (using expressions shown in equations (23), (24) and (25)) are calculated for each set and shown in table (I). For each set, the values of the parameters are chosen so that the neutrino mass eigenvalues follow normal hierarchy and the sum of neutrino masses, Σ is in agreement with its observational value.

Set no.	$M(\text{GeV})$	y_0	$\tilde{m}(\text{eV})$	γ_ν	β_ν	\hat{A}_ν (eV)	\hat{B}_ν (eV)	\hat{C}_ν (eV)	Σ (eV)
I	4×10^{11}	0.0201	0.043379	57.32°	343.95°	-0.317	-0.177	0.461	0.0614
II	2×10^{11}	0.0201	0.074759	171.97°	171.97°	1.507	0.733	0.231	0.0684
III	8×10^{10}	0.0049	0.022743	343.95°	57.32°	2.172	0.692	1.528	0.0644
IV	4×10^{10}	0.0048	0.031625	57.32°	114.65°	0.827	0.669	0.796	0.0645

TABLE I: Neutrino mass matrix elements for different values of right-handed neutrino mass M . These values are used to estimate the CP asymmetry and wash-out parameters.

For the hierarchical mass spectrum of light neutrinos, the renormalization group running between low energy and the high energy seesaw scale has a nominal impact on the neutrino parameters, except from an overall scaling of the light neutrino masses [38–40]. The effect of scaling can be taken care of by multiplying by a factor of 1.2 in the low energy values of

the parameters [41].

The purpose of setting up these benchmark points is to determine and compare the production baryon asymmetry via unflavoured and two-flavoured leptogenesis. Hence, wash-out parameter $K = \frac{\tilde{m}}{m_*} = \frac{y_0^2(1+r^2)v^2}{Mm_*}$ and the CP asymmetries ϵ , ϵ_a , and ϵ_τ are calculated corresponding to different M values. For each set, baryon asymmetry is calculated via both unflavoured and two-flavoured leptogenesis. For the purpose of having a comparative study, we have kept the values of washout parameter K and the CP asymmetry parameter $\epsilon(\epsilon_i)$ consistent for the study of unflavoured and two-flavoured leptogenesis. The consistency is ensured by the relation $\epsilon = \epsilon_a + \epsilon_\tau$. In case of two-flavoured leptogenesis, the flavour projection operators K_0^i , expressed in Eq.(34), are calculated as

$$K_0^a = \frac{(Y^*)_{e1}(Y)_{e1}}{(Y^\dagger Y)_{11}} + \frac{(Y^*)_{\mu 1}(Y)_{\mu 1}}{(Y^\dagger Y)_{11}} = \frac{r^2}{1+r^2}, \quad (45)$$

and

$$K_0^\tau = \frac{(Y^*)_{\tau 1}(Y)_{\tau 1}}{(Y^\dagger Y)_{11}} = \frac{1}{1+r^2}, \quad (46)$$

for each benchmark set.

The flavour independent, as well as flavour-specific CP asymmetry parameters arising from the model, mentioned in equations (38 - 39), respectively, are functions of the neutrino mass eigenvalues m_1, m_2, m_3 through the neutrino mass matrix elements $\hat{A}_\nu, \hat{B}_\nu, \hat{C}_\nu$. The mass eigenvalues m_2, m_3 and thereby the elements $\hat{A}_\nu, \hat{B}_\nu, \hat{C}_\nu$ are calculated using the equations (22- 25) for different values of m_1 . The allowed ranges of x_ν and y_ν , given in Eq.(29), are used to estimate the CP asymmetry parameters.

The suitable set of Boltzmann equations are solved numerically and they are shown in the appendix(E). The final lepton asymmetries thus obtained are used to calculate the final baryon asymmetries. The final results corresponding to different sets are enlisted in table (II) and table (III), for unflavoured and two-flavoured leptogenesis, respectively. The corresponding plots are shown in Fig.(6) in the appendix (E). The baryon asymmetries $|\eta_B|$ are compared in table (IV) to realize the enhancement in the result after considering leptogenesis in an appropriate flavoured regime.

In addition to using the benchmark points, to observe the importance of the flavour effects in producing baryon asymmetry through unflavoured and two-flavoured leptogenesis, we numerically vary the right-handed neutrino mass M values in the range $[2 - 6] \times 10^{10}$ GeV, for different values of K and ϵ (K, K_0^i and ϵ_i for flavoured leptogenesis) and show the

Set no.	$M(\text{GeV})$	K	ϵ	$ \eta_B /10^{-10}$
I	4×10^{11}	43.379	-3.45×10^{-6}	1.78
II	2×10^{11}	74.759	6.12×10^{-6}	1.67
III	8×10^{10}	22.473	4.73×10^{-7}	0.54
IV	4×10^{10}	31.625	1.42×10^{-6}	1.07

TABLE II: Baryon asymmetries from unflavoured leptogenesis for different values of M and K .

Set no.	$M(\text{GeV})$	K	ϵ_a	ϵ_τ	K_0^a	K_0^τ	$ \eta_B /10^{-10}$
I	4×10^{11}	43.379	5.43×10^{-7}	-3.99×10^{-6}	0.294911	0.705088	2.02
II	2×10^{11}	74.759	9.61×10^{-7}	5.16×10^{-6}	0.181698	0.818301	5.10
III	8×10^{10}	22.473	4.19×10^{-7}	5.38×10^{-8}	0.588344	0.411655	1.56
IV	4×10^{10}	31.625	4.28×10^{-7}	9.92×10^{-7}	0.429678	0.570321	3.26

TABLE III: Baryon asymmetries from two-flavoured leptogenesis for different values of M , K , ϵ_i and K_0^i .

results in Fig.(3). In Fig.(3), baryon asymmetries are plotted against M . After eliminating the results showing over-production of baryon asymmetry $|\eta_B|$, it shows that within the experimental bound $(4.7 - 6.5) \times 10^{-10}$, the results coming from two-flavoured leptogenesis are enhanced over the results coming from unflavoured leptogenesis.

IV. RELATING CP VIOLATION IN LOW AND HIGH ENERGY PHENOMENA

Baryogenesis through leptogenesis can easily be implemented in the seesaw models. CP violation in lepton sector which are measurable in low-energy experiments like neutrino factories can have profound consequences in high-energy phenomena like leptogenesis. It is believed that the CP violation in the two sectors is in general not related to each other. The difficulty in setting up the relation is due to lack of low-energy data available to quantify the parameters of the seesaw model. There are interesting studies [42] which show that it may be possible in specific Grand Unification inspired models up to size and sign of the observed BAU to CP violation at low energies. The link between CP violations in leptogenesis and

$M(\text{GeV})$	$ \eta_B $ from unflavoured leptogenesis	$ \eta_B $ from two-flavoured leptogenesis
4×10^{11}	1.78×10^{-10} [Set-I, 6a]	2.02×10^{-10} [Set-I, 6b]
2×10^{11}	1.67×10^{-10} [Set-II, 6c]	5.10×10^{-10} [Set-II, 6d]
8×10^{10}	5.38×10^{-11} [Set-III, 6e]	1.56×10^{-10} [Set-III, 6f]
4×10^{10}	1.07×10^{-10} [Set-IV, 6g]	3.26×10^{-10} [Set-IV, 6h]

TABLE IV: Baryon asymmetries from unflavoured and two-flavoured leptogenesis for different values of M , and $\epsilon(\epsilon_i)$. We have shown a comparative study on how the flavour effects enhance the baryon asymmetry. The different sets in the table correspond to the corresponding plots, where the set of Boltzmann equations are numerically solved and lepton asymmetries are shown.

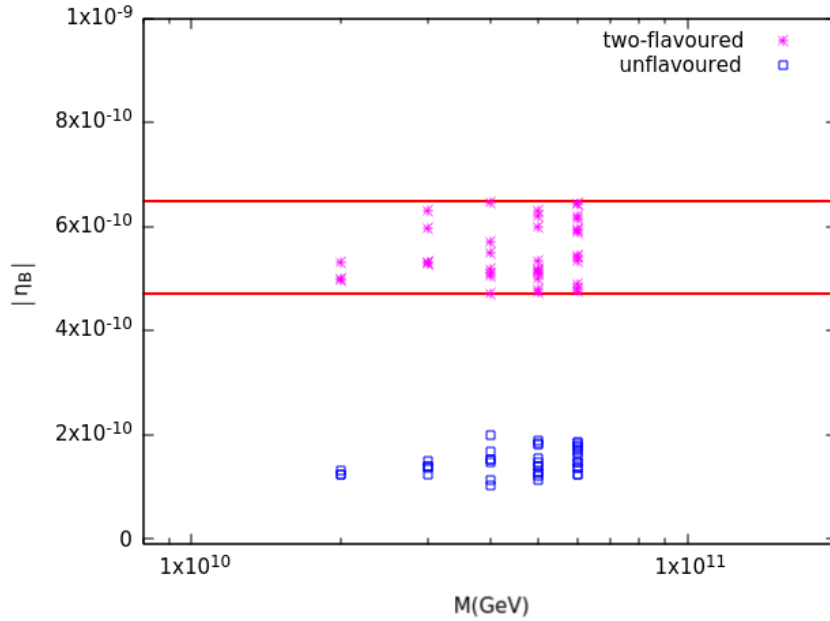


FIG. 3: Comparing the Baryon asymmetry results coming from unflavoured and two-flavoured leptogenesis regimes. The blue points correspond to baryon asymmetries via unflavoured leptogenesis. On the other hand, the magenta points correspond to baryon asymmetries via two-flavoured leptogenesis. The region between the two red lines signifies the experimentally obtained range of baryon asymmetry, i.e. $[4.7 - 6.5] \times 10^{-10}$.

low-energy observable like neutrino less double beta decay, lepton flavour violation, Jarlskog invariant has been studied in [43–54]. In our work, we encounter a common origin of CP

violation in low-energy neutrino experiments in terms of J_{CP} and in high-energy sector in terms of CP asymmetry parameter, required for leptogenesis. It can be explained in a geometrical interpretation of CP violation with Majorana neutrinos.

Analogous to the CKM matrix in the quark sector, in the lepton sector, six unitarity triangles can be formed known as leptonic unitarity triangles, from the orthogonality of the rows and columns of the 3×3 PMNS matrix. These triangles are analogous to the quark unitarity triangles used for studying various manifestations of CP violation. However, in the case of Majorana neutrinos, there is an important difference which will be discussed here. The unitarity condition of V is given by,

$$V^\dagger V = V V^\dagger = 1. \quad (47)$$

Under the rephasing transformation of lepton fields $L_\alpha \rightarrow e^{i\phi_\alpha} L_\alpha$, the matrix V transforms as $V_{\alpha i} \rightarrow V'_{\alpha i} = e^{i\phi_\alpha} V_{\alpha i}$. The vector $V_{\alpha i} V_{\beta i}^* \rightarrow e^{i(\phi_\alpha - \phi_\beta)} V_{\alpha i} V_{\beta i}^*$ rotates in the complex plane, whereas the vector $V_{\alpha i} V_{\alpha j}^*$ remains invariant. Based on this observation, the unitarity triangles are classified into Dirac triangles and Majorana triangles which are discussed below.

A. Dirac Unitarity Triangles

From the orthogonality of rows of the mixing matrix V ,

$$\sum V_{\alpha i} V_{\beta i}^* = 0 \quad (\alpha \neq \beta), \quad (48)$$

we obtain the expressions of three Dirac triangles,

$$T_{e\mu} : V_{e1} V_{\mu 1}^* + V_{e2} V_{\mu 2}^* + V_{e3} V_{\mu 3}^* = 0, \quad (49)$$

$$T_{e\tau} : V_{e1} V_{\tau 1}^* + V_{e2} V_{\tau 2}^* + V_{e3} V_{\tau 3}^* = 0, \quad (50)$$

$$T_{\mu\tau} : V_{\mu 1} V_{\tau 1}^* + V_{\mu 2} V_{\tau 2}^* + V_{\mu 3} V_{\tau 3}^* = 0. \quad (51)$$

The orientation of the Dirac triangles has no physical significance since under the rephasing of the charged-lepton fields these triangles exhibit rotation in the complex plane. The Dirac triangles share a common area $A = \frac{1}{2} J_{CP}$ and the vanishing area of the Dirac triangles indicates vanishing Jarlskog Invariant $J_{CP} = 0$ but it does not guarantee the conservation of CP symmetry. It only indicates that the Dirac CP phase is zero, but the two Majorana

phases can still violate CP. Thus Dirac triangles fail to completely describe CP violation [55].

Nevertheless, the quantity J_{CP} can be determined through

$$J_{CP} = \text{Im} (V_{11}V_{22}V_{12}^*V_{21}^*), \quad (52)$$

by using the explicit form of V . In this case, it is not possible to get a compact form of J_{CP} , we make an approximate analytical study in appendix(D), which shows that it depends on the phases β_ν and γ_ν . Also, it can be observed from equations (38) and (39), the same phases appear in the CP asymmetry parameter. We numerically calculate the values of J_{CP} and ϵ as shown in Fig.(4). In order to calculate ϵ the value of m_1 is chosen to be 0.021 eV, and

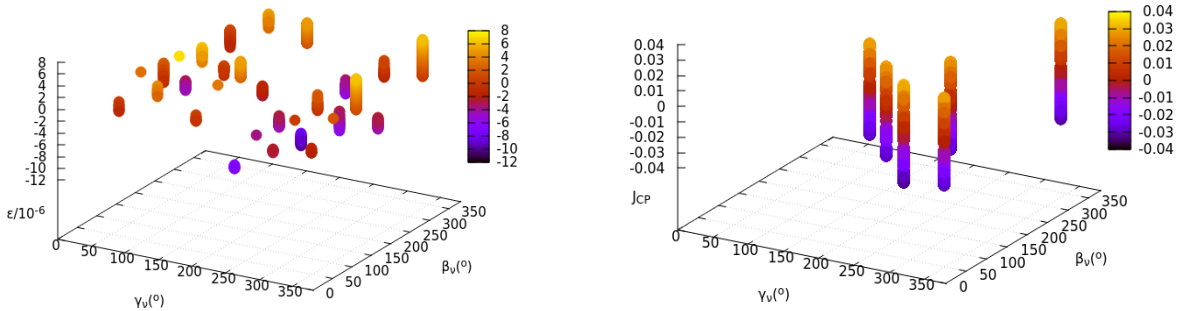


FIG. 4: 3D scattered plots of ϵ and J_{CP} as function of β_ν and γ_ν : The figure on the left shows the high-energy CP violation measured by CP asymmetry ϵ as a function of phases γ_ν and β_ν in a unit of 10^{-6} , and the figure in right shows the low-energy CP violation measured by Jarlskog invariant J_{CP} as a function of γ_ν and β_ν . These plots show the common connection between low- and high-energy CP violation through the two phases (γ_ν, β_ν) appearing in the neutrino mass matrix.

m_2 and m_3 are further calculated following the relation given in Eq.(13), using the allowed parameter space for $[x_\nu, y_\nu]$ given in Eq.(29). The allowed neutrino mass eigenvalues m_1, m_2, m_3 are found by imposing the bound on total neutrino mass $\Sigma = m_1 + m_2 + m_3 < 0.12$ eV. The parameter y_0 is varied in the range $[0.0101 : 0.0201]$. The right-handed neutrino mass M is chosen to be 8×10^{10} GeV. The phases $[\gamma_\nu, \beta_\nu]$ are both varied in the range $[0 : 2\pi]$. The maximum order of the obtained CP asymmetry is found to be $|\epsilon| \sim 10^{-5}$.

On the other hand, in the expression of J_{CP} in Eq.(52), the mixing matrix V is a function of U_ν , U_l and phases (θ, ϕ, ψ) as it can be seen in Eq.(11). Here U_ν and U_l are given in appendix (A) and (B), respectively. The elements of $U_l(U_\nu)$ are functions of charged (neutral) lepton mass ratios $[x_l(x_\nu), y_l(y_\nu)]$. The charged lepton mass ratios are determined, as given in Eq.(14). Also keeping in mind the factorization of lepton mass matrices given in Eq.(8), can be written, when the condition imposed on elements of the neutrino mass matrix given in Eq.(7) was $\arg(1 + \hat{A}_\nu e^{i\gamma_\nu}) = 2\arg(r + \hat{B}_\nu e^{i\beta_\nu})$. Using this condition one can see ψ_ν is related to the phases $[\gamma_\nu, \beta_\nu]$ as,

$$\frac{\hat{A}_\nu \sin \gamma_\nu}{1 + \hat{A}_\nu \cos \gamma_\nu} = \tan 2\psi_\nu, \quad \frac{\hat{B}_\nu \sin \beta_\nu}{r + \hat{B}_\nu \cos \beta_\nu} = \tan \psi_\nu. \quad (53)$$

Therefore, it is understood that J_{CP} is a function of the phases $[\gamma_\nu, \beta_\nu]$ through ψ_ν . Since, \hat{A}_ν , \hat{B}_ν , \hat{C}_ν and r depend on M , m_1 , m_2 , m_3 and y_0 , we vary $m_1 \sim [0.001 - 0.05]\text{eV}$ and $y_0 \sim [0.0001 - 1]$ and obtained m_2 , m_3 using Eq.(13) within the allowed parameter space for $[x_\nu, y_\nu]$ mentioned in Eq.(29). We also varied θ , ϕ , ψ_l and $[\gamma_\nu, \beta_\nu]$ in the range $[0 : 2\pi]$, and determined the allowed range for ψ_ν and thereby for $[\gamma_\nu, \beta_\nu]$, which satisfy the conditions given in Eq.(53) for obtaining a scattered plot of J_{CP} as a function of $[\gamma_\nu, \beta_\nu]$. The maximum low energy CP violation through $|J_{CP}|$ for $M = 8 \times 10^{10} \text{ GeV}$ is found to be ~ 0.032 .

B. Majorana Unitarity Triangles

From the orthogonality of columns of the mixing matrix, V ,

$$\Sigma V_{\alpha i} V_{\alpha j}^* = 0 \quad (i \neq j), \quad (54)$$

we obtain the expressions of three Majorana triangles,

$$T_{12} : V_{e1} V_{e2}^* + V_{\mu 1} V_{\mu 2}^* + V_{\tau 1} V_{\tau 2}^* = 0, \quad (55)$$

$$T_{13} : V_{e1} V_{e3}^* + V_{\mu 1} V_{\mu 3}^* + V_{\tau 1} V_{\tau 3}^* = 0, \quad (56)$$

$$T_{23} : V_{e2} V_{e3}^* + V_{\mu 2} V_{\mu 3}^* + V_{\tau 2} V_{\tau 3}^* = 0. \quad (57)$$

Since the Majorana triangles remain invariant under the rephasing, the orientation of the Majorana triangles has physical significance. These Majorana triangles provide the necessary and sufficient conditions for CP conservation in the lepton sector. The absence of CP violation is guaranteed by

1. Vanishing of the common area $A = \frac{1}{2}J_{CP}$ of the Majorana triangles.
2. Orientation of all Majorana triangles along the direction of the real or imaginary axes.

The first condition implies that the three triangles collapse into lines in the complex plane and the vanishing of the Dirac phase. The second condition implies that the Majorana phases do not violate CP. Hence the three Majorana triangles are capable to provide a complete description of CP violation, unlike the Dirac triangles. If each one of the sides of the Majorana triangles is not parallel to one of the axes, then it is a signal for CP non-conservation, contrarily to the Dirac triangle case where only a nonzero area signifies CP violation [55].

The low energy CP violation can be obtained through the lepton unitarity triangles as discussed earlier. We consider the Majorana triangle, T_{13} as expressed in Eq.(56), and define a parameter Z as a side of the Majorana triangle- T_{13} after resizing it so that the base of the triangle becomes of unit length. In analogy with the quark sector, the triangle corresponding to the unitary conditions in the first and third columns with proper rescaling is shown in a figure in NuFIT 5.0 [23]. The figure indicates the absence of CP violation would imply a flat triangle i.e., $\text{Im}(Z) = 0$, where

$$Z = -\frac{V_{e1}V_{e3}^*}{V_{\mu1}V_{\mu3}^*} = \text{Re}(Z) + i \text{Im}(Z). \quad (58)$$

As long as the area of the triangle is non-zero and all Majorana triangles are oriented along neither real nor imaginary axes, the CP symmetry will be violated. In order to understand the dependence of the low energy CP violation through the Z -parameter, on the CP violating phases arising in the neutrino mass matrix, the real and imaginary counterpart of Z -parameter is plotted as functions of the two phases (γ_ν, β_ν) as depicted in Fig.(5). Here, the mixing matrix V is found from the Eq.(11). From the Eq.(53), it can be seen that Z -parameter is a function of the phases $[\gamma_\nu, \beta_\nu]$ through ψ_ν .

For right-handed neutrino mass $M = 8 \times 10^{10}$ GeV, we varied $m_1 \sim [0.001 - 0.05]$ eV and $y_0 \sim [0.0001 - 1]$ and obtained m_2, m_3 through Eq.(13) within the allowed parameter space for $[x_\nu, y_\nu]$ given in Eq.(29). We also varied θ, ϕ, ψ_l and $[\gamma_\nu, \beta_\nu]$ in the range $[0 : 2\pi]$, and determined the allowed range for ψ_ν and thereby for $[\gamma_\nu, \beta_\nu]$ which satisfy the conditions given in Eq.(53) for obtaining a scattered plot of $\text{Re}(Z)$ and $\text{Im}(Z)$ as a function of $[\gamma_\nu, \beta_\nu]$.

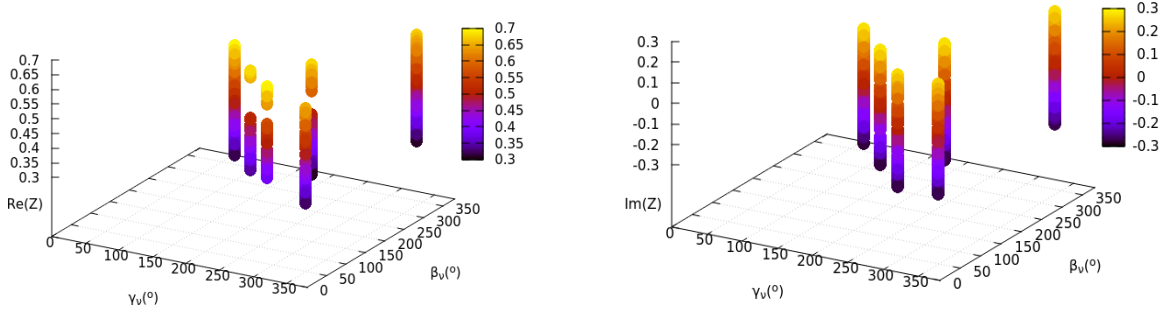


FIG. 5: 3D scattered plots of $\text{Re}(Z)(\gamma_\nu, \beta_\nu)$ and $\text{Im}(Z)(\gamma_\nu, \beta_\nu)$: The plots show the dependence of the Z -parameter on the CP violating phases arising in the neutrino mass matrix, for the case of Majorana triangle- T_{13} (Eq.(56)). The figure in left(right) shows $\text{Re}(Z)(\text{Im}(Z))$ as functions of the two phases (γ_ν, β_ν) appearing in neutrino mass matrix.

V. CONCLUSION

In the minimal extension of the SM with right-handed neutrinos and scalar triplet, baryogenesis can be achieved through leptogenesis from the CP violating decay of either the lightest right-handed neutrino or triplet scalar. We have studied a minimal type-II seesaw model where the SM is extended with one right-handed neutrino and one triplet scalar. There are two mass scales involved in this case; the mass of the right-handed neutrino, M , and that of the triplet scalar, M_Δ . Considering there are no heavy scalars in the theory we choose to work in the hierarchical mass $M \ll M_\Delta$. In this case, for leptogenesis, the sources of CP violation can be found, that are mediated by the decay of the heavy right-handed neutrino. In the absence of extra right-handed neutrinos, non-vanishing CP asymmetry is sourced from the interference of the tree-level and one-loop diagrams mediated by the Higgs triplet scalar, which is taken to be heavier than the right-handed neutrino. By lowering the mass scale of the heavy right-handed neutrino, its mass is taken to be in the range $M \subset [10^{10}, 10^{11}]$ GeV for successful baryogenesis via leptogenesis. In this mass range, we have studied the leptogenesis in a two-flavoured regime. It is seen that for $M \subset [10^{10}, 10^{11}]$ GeV, the obtained lepton asymmetries lead to baryon asymmetry within the desired range of $\eta_B \sim (4.7 - 6.5) \times 10^{-10}$. We show that incorporating appropriate flavour consideration,

the results show an enhancement in the baryon asymmetry as compared to unflavoured case. Thus the minimal type-II seesaw model with only one heavy right-handed neutrino and one heavier Higgs triplet scalar can provide a viable explanation for neutrino mass generation and baryon asymmetry of the Universe through leptogenesis. We show this feature by using the Fritzsch-type texture. Using geometrical interpretation of low-energy CP violation we also show there is a common link between CP violation of both low- and high-energy regimes. These features can further be implemented in more predictive models like left-right symmetric models.

Appendix A: Diagonalizing neutrino mass matrix m_ν with two-zero texture

The elements of the matrix U_ν are given in terms of the ratios x_ν, y_ν :

$$\begin{aligned}
U_{\nu 11} &= i \left[\frac{1}{(1+x_\nu)(1-x_\nu^2 y_\nu^2)} \right]^{\frac{1}{2}}, \\
U_{\nu 12} &= + \left[\frac{x_\nu(1-y_\nu-x_\nu y_\nu)}{(1+x_\nu)(1-y_\nu)(1-x_\nu y_\nu)} \right]^{\frac{1}{2}}, \\
U_{\nu 13} &= + \left[\frac{x_\nu^2 y_\nu^3}{(1-y_\nu)(1-x_\nu^2 y_\nu^2)} \right]^{\frac{1}{2}}, \\
U_{\nu 21} &= -i \left[\frac{x_\nu}{(1+x_\nu)(1+x_\nu y_\nu)} \right]^{\frac{1}{2}}, \\
U_{\nu 22} &= + \left[\frac{(1-y_\nu-x_\nu y_\nu)}{(1+x_\nu)(1-y_\nu)} \right]^{\frac{1}{2}}, \\
U_{\nu 23} &= + \left[\frac{x_\nu y_\nu}{(1-y_\nu)(1+x_\nu y_\nu)} \right]^{\frac{1}{2}}, \\
U_{\nu 31} &= +i \left[\frac{x_\nu^2 y_\nu(1-y_\nu-x_\nu y_\nu)}{(1+x_\nu)(1-x_\nu^2 y_\nu^2)} \right]^{\frac{1}{2}}, \\
U_{\nu 32} &= - \left[\frac{x_\nu y_\nu}{(1+x_\nu)(1-y_\nu)(1-x_\nu y_\nu)} \right]^{\frac{1}{2}}, \\
U_{\nu 33} &= + \left[\frac{1-y_\nu-x_\nu y_\nu}{(1-y_\nu)(1-x_\nu^2 y_\nu^2)} \right]^{\frac{1}{2}}.
\end{aligned}$$

Appendix B: Diagonalizing charged-lepton mass matrix m_l with three-zero texture

The elements of the matrix U_l are given in terms of the ratios x_l, y_l :

$$\begin{aligned}
U_{l11} &= + \left[\frac{1 - y_l}{(1 + x_l)(1 - x_ly_l)(1 - y_l + x_ly_l)} \right]^{\frac{1}{2}}, \\
U_{l12} &= -i \left[\frac{x_l(1 + x_ly_l)}{(1 + x_l)(1 + y_l)(1 - y_l + x_ly_l)} \right]^{\frac{1}{2}}, \\
U_{l13} &= + \left[\frac{x_ly_l^3(1 - x_l)}{(1 - x_ly_l)(1 + y_l)(1 - y_l + x_ly_l)} \right]^{\frac{1}{2}}, \\
U_{l21} &= + \left[\frac{x_l(1 - y_l)}{(1 + x_l)(1 - x_ly_l)} \right]^{\frac{1}{2}}, \\
U_{l22} &= +i \left[\frac{1 + x_ly_l}{(1 + x_l)(1 + y_l)} \right]^{\frac{1}{2}}, \\
U_{l23} &= + \left[\frac{y_l(1 - x_l)}{(1 - x_ly_l)(1 + y_l)} \right]^{\frac{1}{2}}, \\
U_{l31} &= - \left[\frac{x_ly_l(1 - x_l)(1 + x_ly_l)}{(1 + x_l)(1 - x_ly_l)(1 - y_l + x_ly_l)} \right]^{\frac{1}{2}}, \\
U_{l32} &= -i \left[\frac{y_l(1 - x_l)(1 - y_l)}{(1 + x_l)(1 + y_l)(1 - y_l + x_ly_l)} \right]^{\frac{1}{2}}, \\
U_{l33} &= + \left[\frac{(1 - y_l)(1 + x_ly_l)}{(1 - x_ly_l)(1 + x_l)(1 - y_l + x_ly_l)} \right]^{\frac{1}{2}}.
\end{aligned}$$

Appendix C: The importance of flavour projectors in leptogenesis

Before deepening the elaborate execution of flavoured leptogenesis, we will see how lepton flavours play a role in constructing CP asymmetry. In general, in the case of leptogenesis, CP violation can be observed from N_1 decay in two cases:

1. If the rate of production of leptons and anti-leptons differ, expressed as

$$\Gamma \neq \bar{\Gamma},$$

where Γ is the decay rate of the process $N_1 \longrightarrow l + \phi^\dagger$, and $\bar{\Gamma}$ is the decay rate of the process $N_1 \longrightarrow \bar{l}' + \phi$. The CP asymmetry can be expressed in terms of these decay rates, as

$$\epsilon = \frac{\Gamma - \bar{\Gamma}}{\Gamma + \bar{\Gamma}}. \quad (\text{C1})$$

2. If the lepton flavour effects are included, it can affect the CP asymmetry construction in two ways,

- (a) It suppresses the washout, as the interaction of the leptons with Higgs, during inverse decay, gets fragmented in terms of different flavour states. In this context, we define a parameter called flavour projector[28, 32, 56, 57],

$$K_i = |\langle l | l_i \rangle|^2 = \frac{\Gamma_i}{\Gamma}, \quad i = e, \mu, \tau$$

and

$$\bar{K}_i = |\langle \bar{l}' | \bar{l}_i \rangle|^2 = \frac{\bar{\Gamma}_i}{\bar{\Gamma}}.$$

Here, Γ_i is the partial decay rate of the process $N_1 \rightarrow l_i + \phi^\dagger$, and $\bar{\Gamma}_i$ is the partial decay rate of the process $N_1 \rightarrow \bar{l}_i + \phi$. The concept of total decay rate $\Gamma = \sum_i \Gamma_i$, and $\bar{\Gamma} = \sum_i \bar{\Gamma}_i$ leads to the realisation that $\sum_i K_i = \sum_i \bar{K}_i = 1$. Due to these flavour effects, we need to consider individually flavoured CP asymmetries as

$$\epsilon_i = \frac{\Gamma_i - \bar{\Gamma}_i}{\Gamma_i + \bar{\Gamma}_i}. \quad (\text{C2})$$

- (b) If the state $|\bar{l}'\rangle$ is not the CP conjugate state of the state $|l\rangle$, which arises from misalignment in the flavour space due to loop-effects, then it gives an additional source of CP violation. To understand this effect, we introduce projector difference, as

$$\Delta K_i = K_i - \bar{K}_i.$$

The CP asymmetry can be further modified, incorporating $K_i = K_0^i + \frac{\Delta K_i}{2}$ and $\bar{K}_i = K_0^i - \frac{\Delta K_i}{2}$, as

$$\epsilon_i \sim \epsilon K_0^i + \frac{\Delta K_i}{2}. \quad (\text{C3})$$

Here, $K_0^i = \frac{K_i + \bar{K}_i}{2}$ is the tree level contributions to the projections.

In the Eq.(C3), the first term on the right-hand side, proportional to ϵ , comes from the type of contribution discussed in the first case. On the other hand, the second term proportional to ΔK_i comes from the contribution mentioned in the second case, as the term vanishes when we have $|\bar{l}'\rangle$ as the CP conjugate state of $|l\rangle$. From Eq.(C3), it can be easily shown that $\epsilon = \sum_i \epsilon_i$. As we are particularly interested in a temperature range where lepton flavour interaction becomes important, we have incorporated flavour projectors, especially the tree

level contribution K_0^i in the flavoured Boltzmann equations, which we have described in the next section. Flavour projectors become important to segregate the flavour regimes of leptogenesis in terms of lepton flavour alignment or non-alignment. In the context of our chosen temperature range, the lepton flavour non-alignment problem will be relevant, which refers to the situation when no flavour state can be found to be perfectly aligned with the states $|l\rangle$ and $|l'\rangle$ [28].

When only the τ -Yukawa processes are in thermal equilibrium, then the concept of flavour projectors suggests,

$$\sum_{i=a,\tau} K_i = K_a + K_\tau = 1,$$

and

$$\sum_{i=a,\tau} \bar{K}_i = \bar{K}_a + \bar{K}_\tau = 1,$$

where, $|l_a\rangle$ and $|\bar{l}_a\rangle$ are two entangled states of flavours e and μ . Generally, this condition appears as a two-flavoured leptogenesis scenario. On the other hand, when τ and μ -Yukawa processes are in thermal equilibrium, no entangled flavour states can be formed. The thermal bath becomes populated with the CP-conjugate flavour states $|l_i\rangle$ and $|\bar{l}_i\rangle$ (with $i = e, \mu, \tau$). Here arises typically the case of three-flavoured or fully-flavoured leptogenesis. From the flavour projector condition, we obtain,

$$\sum_{i=e,\mu,\tau} K_i = K_e + K_\mu + K_\tau = 1,$$

and

$$\sum_{i=e,\mu,\tau} \bar{K}_i = \bar{K}_e + \bar{K}_\mu + \bar{K}_\tau = 1.$$

Appendix D: Low scale CP violation and Jarlskog invariant J_{CP}

In simplified form,

$$J_{CP} \sim \text{Im} [V_{13}], \quad (\text{D1})$$

where V_{13} can be obtained from Eq.(11) as,

$$V_{13} = U_{l11} U_{\nu13}^* e^{i\theta} + U_{l21} U_{\nu23}^* e^{i\phi} + U_{l31} U_{\nu33}^* e^{i\psi}. \quad (\text{D2})$$

From appendix(A), it is clear that U_{l11} , U_{l21} , U_{l31} , $U_{\nu13}$, $U_{\nu23}$, $U_{\nu33}$ are all real, and U_{l11} , U_{l21} , U_{l31} are function of $x_l = \frac{m_e}{m_\nu}$, $y_l = \frac{m_\mu}{m_\tau}$. Since, the charged lepton masses are already

known, the ratios x_l and y_l have definite values, and so the values of U_{l11} , U_{l21} , U_{l31} are also known. Hence, after further simplification of equations (D1) and (D2), we obtain

$$J_{CP} \sim U_{l11}U_{\nu13} \sin \theta + U_{l21}U_{\nu23} \sin \phi + U_{l31}U_{\nu33} \sin \psi. \quad (D3)$$

Leading from the definition of x_ν and y_ν given in Eq.(13) and combining equations (23), (24), and (25), the parameters $U_{\nu13}$, $U_{\nu23}$, $U_{\nu33}$ can be written as functions of the two arbitrary CP violating phases γ_ν and β_ν (introduced in Eq.(7)) as $U_{\nu13} \rightarrow g_1(\gamma_\nu, \beta_\nu)$, $U_{\nu23} \rightarrow g_2(\gamma_\nu, \beta_\nu)$ and $U_{\nu33} \rightarrow g_3(\gamma_\nu, \beta_\nu)$. Hence,

$$J_{CP} \sim U_{l11}g_1(\gamma_\nu, \beta_\nu) \sin \theta + U_{l21}g_2(\gamma_\nu, \beta_\nu) \sin \phi + U_{l31}g_3(\gamma_\nu, \beta_\nu) \sin \psi. \quad (D4)$$

The functions $g_1(\gamma_\nu, \beta_\nu)$, $g_2(\gamma_\nu, \beta_\nu)$, $g_3(\gamma_\nu, \beta_\nu)$ are given by,

$$g_1(\gamma_\nu, \beta_\nu) = r(f_1 - f_2) \left[\frac{1}{2f_1f_2(f_1 + f_2 - 2r^2)} \right]^{\frac{1}{2}}, \quad (D5)$$

$$g_2(\gamma_\nu, \beta_\nu) = \left[\frac{f_2(f_1^2 - f_2^2)}{2f_1f_2(f_1 + f_2 - 2r^2)} \right]^{\frac{1}{2}}, \quad (D6)$$

$$g_3(\gamma_\nu, \beta_\nu) = (f_1 + f_2) \left[\frac{(f_2 - r^2)}{2f_1f_2(f_1 + f_2 - 2r^2)} \right]^{\frac{1}{2}}, \quad (D7)$$

where

$$f_1 \rightarrow f_1(\gamma_\nu, \beta_\nu) = \left[1 + \hat{A}_\nu^2 + 4 \left(r^2 + \hat{B}_\nu^2 + \hat{C}_\nu^2 \right) + 2\hat{A}_\nu \cos \gamma_\nu + 8r\hat{B}_\nu \cos \beta_\nu \right]^{\frac{1}{2}}, \quad (D8)$$

and

$$f_2 \rightarrow f_2(\gamma_\nu) = \left[1 + \hat{A}_\nu^2 + 2\hat{A}_\nu \cos \gamma_\nu \right]^{\frac{1}{2}}. \quad (D9)$$

Appendix E: Numerical solution of Boltzmann Equations

The solutions of the set of Boltzmann equations are depicted in the figures below (Fig.(6)).

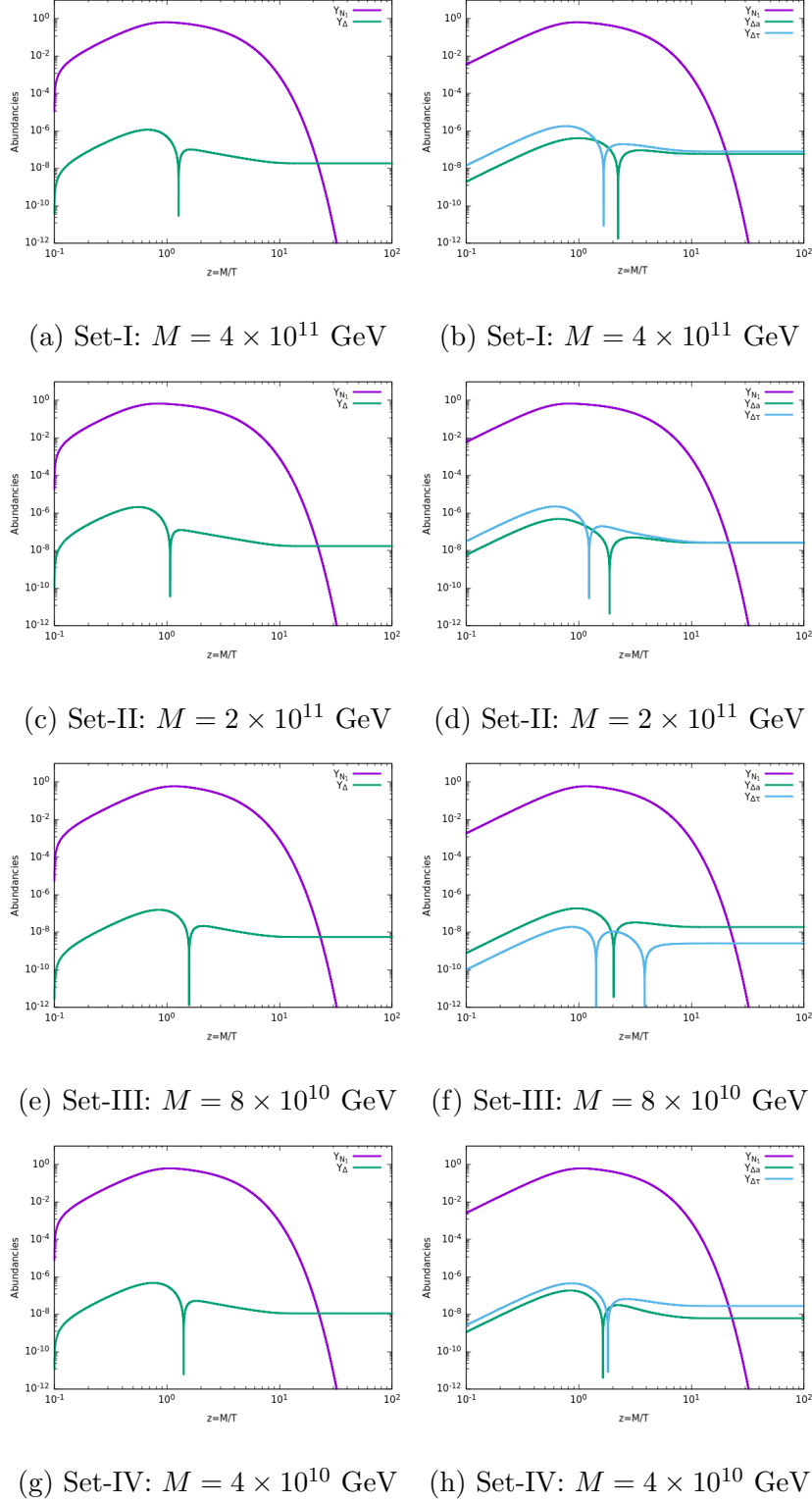


FIG. 6: Evolution of lepton asymmetries for different choices of right-handed neutrino mass M , in unflavoured (left column) and two-flavoured (right column) leptogenesis regimes.

-
- [1] C. Giunti and C. W. Kim, *Fundamentals of Neutrino Physics and Astrophysics* (2007).
 - [2] M. Fukugita and T. Yanagida, Phys. Lett. B **174**, 45 (1986).
 - [3] R. N. Mohapatra and J. C. Pati, Phys. Rev. D **11**, 2558 (1975).
 - [4] G. Senjanovic and R. N. Mohapatra, Phys. Rev. D **12**, 1502 (1975).
 - [5] G. Senjanovic, Nucl. Phys. B **153**, 334 (1979).
 - [6] J. C. Pati and A. Salam, Phys. Rev. D **10**, 275 (1974), [Erratum: Phys.Rev.D 11, 703–703 (1975)].
 - [7] H. Georgi, AIP Conf. Proc. **23**, 575 (1975).
 - [8] H. Fritzsch and P. Minkowski, Annals Phys. **93**, 193 (1975).
 - [9] A. D. Sakharov, Pisma Zh. Eksp. Teor. Fiz. **5**, 32 (1967).
 - [10] T. Hambye and G. Senjanovic, Phys. Lett. B **582**, 73 (2004), arXiv:hep-ph/0307237 .
 - [11] H. Fritzsch, Nucl. Phys. B **155**, 189 (1979).
 - [12] Z.-z. Xing, Phys. Lett. B **550**, 178 (2002), arXiv:hep-ph/0210276 .
 - [13] M. Fukugita, M. Tanimoto, and T. Yanagida, Phys. Lett. B **562**, 273 (2003), arXiv:hep-ph/0303177 .
 - [14] Z.-z. Xing and S. Zhou, Phys. Lett. B **606**, 145 (2005), arXiv:hep-ph/0411044 .
 - [15] H. Fritzsch, Z.-z. Xing, and S. Zhou, JHEP **09**, 083 (2011), arXiv:1108.4534 [hep-ph] .
 - [16] H. Borgohain, M. K. Das, and D. Borah, JHEP **06**, 064 (2019), arXiv:1904.02484 [hep-ph] .
 - [17] C. D. Froggatt and H. B. Nielsen, Nucl. Phys. B **147**, 277 (1979).
 - [18] A. Abada, S. Davidson, A. Ibarra, F. X. Josse-Michaux, M. Losada, and A. Riotto, JHEP **09**, 010 (2006), arXiv:hep-ph/0605281 .
 - [19] R. Gatto, G. Sartori, and M. Tonin, Phys. Lett. B **28**, 128 (1968).
 - [20] P.-H. Gu, H. Zhang, and S. Zhou, Phys. Rev. D **74**, 076002 (2006), arXiv:hep-ph/0606302 .
 - [21] Z.-z. Xing and H. Zhang, Phys. Lett. B **569**, 30 (2003), arXiv:hep-ph/0304234 .
 - [22] H. Nishiura, K. Matsuda, and T. Fukuyama, Phys. Rev. D **60**, 013006 (1999), arXiv:hep-ph/9902385 .
 - [23] I. Esteban, M. C. Gonzalez-Garcia, M. Maltoni, T. Schwetz, and A. Zhou, JHEP **09**, 178 (2020), arXiv:2007.14792 [hep-ph] .
 - [24] N. Aghanim *et al.* (Planck), Astron. Astrophys. **641**, A6 (2020), [Erratum: Astron.Astrophys.

- 652, C4 (2021)], arXiv:1807.06209 [astro-ph.CO] .
- [25] C. Amsler *et al.* (Particle Data Group), Phys. Lett. B **667**, 1 (2008).
 - [26] A. Strumia, in *Les Houches Summer School on Theoretical Physics: Session 84: Particle Physics Beyond the Standard Model* (2006) pp. 655–680, arXiv:hep-ph/0608347 .
 - [27] S. Y. Khlebnikov and M. E. Shaposhnikov, Nucl. Phys. B **308**, 885 (1988).
 - [28] E. Nardi, Y. Nir, E. Roulet, and J. Racker, JHEP **01**, 164 (2006), arXiv:hep-ph/0601084 .
 - [29] C. S. Fong, E. Nardi, and A. Riotto, Adv. High Energy Phys. **2012**, 158303 (2012), arXiv:1301.3062 [hep-ph] .
 - [30] Y. H. Ahn, S. K. Kang, C. S. Kim, and J. Lee, Phys. Rev. D **77**, 073009 (2008), arXiv:0711.1001 [hep-ph] .
 - [31] E. Nardi, Y. Nir, J. Racker, and E. Roulet, JHEP **01**, 068 (2006), arXiv:hep-ph/0512052 .
 - [32] S. Blanchet and P. Di Bari, JCAP **03**, 018 (2007), arXiv:hep-ph/0607330 .
 - [33] S. Davidson, E. Nardi, and Y. Nir, Phys. Rept. **466**, 105 (2008), arXiv:0802.2962 [hep-ph] .
 - [34] A. Datta, R. Roshan, and A. Sil, (2023), arXiv:2301.10791 [hep-ph] .
 - [35] S. Antusch and S. F. King, Phys. Lett. B **597**, 199 (2004), arXiv:hep-ph/0405093 .
 - [36] S. Antusch, Phys. Rev. D **76**, 023512 (2007), arXiv:0704.1591 [hep-ph] .
 - [37] C. S. Fong, E. Nardi, and A. Riotto, Adv. High Energy Phys. **2012**, 158303 (2012), arXiv:1301.3062 [hep-ph] .
 - [38] P. H. Chankowski and Z. Pluciennik, Phys. Lett. B **316**, 312 (1993), arXiv:hep-ph/9306333 .
 - [39] J. A. Casas, J. R. Espinosa, A. Ibarra, and I. Navarro, Nucl. Phys. B **573**, 652 (2000), arXiv:hep-ph/9910420 .
 - [40] P. H. Chankowski and S. Pokorski, Int. J. Mod. Phys. A **17**, 575 (2002), arXiv:hep-ph/0110249 .
 - [41] S. Antusch, J. Kersten, M. Lindner, and M. Ratz, Nucl. Phys. B **674**, 401 (2003), arXiv:hep-ph/0305273 .
 - [42] G. C. Branco, T. Morozumi, B. M. Nobre, and M. N. Rebelo, Nucl. Phys. B **617**, 475 (2001), arXiv:hep-ph/0107164 .
 - [43] G. C. Branco, R. Gonzalez Felipe, F. R. Joaquim, and M. N. Rebelo, Nucl. Phys. B **640**, 202 (2002), arXiv:hep-ph/0202030 .
 - [44] G. C. Branco and M. N. Rebelo, Nucl. Phys. B Proc. Suppl. **188**, 325 (2009), arXiv:0902.0162 [hep-ph] .

- [45] J. R. Ellis and M. Raidal, Nucl. Phys. B **643**, 229 (2002), arXiv:hep-ph/0206174 .
- [46] T. Endoh, T. Morozumi, and A. Purwanto, Nucl. Phys. B Proc. Suppl. **111**, 291 (2002), arXiv:hep-ph/0201309 .
- [47] P. H. Frampton, S. L. Glashow, and T. Yanagida, Phys. Lett. B **548**, 119 (2002), arXiv:hep-ph/0208157 .
- [48] C. Hagedorn and E. Molinaro, Nucl. Phys. B **919**, 404 (2017), arXiv:1602.04206 [hep-ph] .
- [49] C. Hagedorn, R. N. Mohapatra, E. Molinaro, C. C. Nishi, and S. T. Petcov, Int. J. Mod. Phys. A **33**, 1842006 (2018), arXiv:1711.02866 [hep-ph] .
- [50] A. S. Joshipura, E. A. Paschos, and W. Rodejohann, JHEP **08**, 029 (2001), arXiv:hep-ph/0105175 .
- [51] B. Karmakar and A. Sil, Phys. Rev. D **93**, 013006 (2016), arXiv:1509.07090 [hep-ph] .
- [52] S.-P. Li, Yuan-Yuan-Li, X.-S. Yan, and X. Zhang, Phys. Rev. D **105**, 096008 (2022), arXiv:2201.04977 [hep-ph] .
- [53] K. Moffat, S. Pascoli, S. T. Petcov, and J. Turner, JHEP **03**, 034 (2019), arXiv:1809.08251 [hep-ph] .
- [54] M. N. Rebelo, Phys. Rev. D **67**, 013008 (2003), arXiv:hep-ph/0207236 .
- [55] J. A. Aguilar-Saavedra and G. C. Branco, Phys. Rev. D **62**, 096009 (2000), arXiv:hep-ph/0007025 .
- [56] S. Blanchet, P. Di Bari, and G. G. Raffelt, JCAP **03**, 012 (2007), arXiv:hep-ph/0611337 .
- [57] P. S. B. Dev, P. Di Bari, B. Garbrecht, S. Lavignac, P. Millington, and D. Teresi, Int. J. Mod. Phys. A **33**, 1842001 (2018), arXiv:1711.02861 [hep-ph] .